JOURNAL OF GEOPHYSICAL RESEARCH, VOL. 95, NO. A11, PAGES 18,969–18,980, NOVEMBER 1, 1990

A Survey of Upwelling Ion Event Characteristics

C. J. POLLOCK,[1] M. O. CHANDLER,[1] T. E. MOORE,[1] J. H. WAITE, JR,[2]
C. R. CHAPPELL,[1] AND D. A. GURNETT[3]

Ionospheric ion upwelling in the vicinity of the dayside cleft has been studied, based primarily on data from the Dynamics Explorer 1 spacecraft. Using retarding ion mass spectrometer low-energy ion data and plasma wave instrument dc electric field data, bulk ion plasma parameters, including ion species density and field-aligned bulk velocity and flux, have been derived at points within a number of observed upwelling ion events for the ion species H^+, He^+, O^+, and O^{++}. The ion species bulk parameters near the source latitude are examined and compared. We find that the upwelling plasma is rich in O^+, which typically comprises ~90% of the particle density, followed by H^+ at somewhat less than 10%, and then He^+ and O^{++}, each comprising ~1% of the upwelling ion particle density. The upwelling O^+ ion flux is also commonly dominant over that associated with the other species, with normalized values near the source region which are typically near 10^9 cm^{-2} s^{-1}. The fractional upward H^+ flux is not as small as the fractional H^+ density due to the much larger H^+ upward flow velocities. Integration of the product of the normalized upward ion species flux and the upwelling ion occurrence probability (Lockwood et al., 1985) over the source area yields an estimate of the source strength of this low-altitude cleft region magnetospheric plasma source of 2.6×10^{25} ions s^{-1}.

1. INTRODUCTION

During recent years, it has been consistently demonstrated that the Earth's ionosphere acts as a significant source of magnetospheric plasma [*Shelley et al.*, 1972; *Young et al.*, 1977; *Ghielmetti et al.*, 1978; *Johnson*, 1979; *Balsiger et al.*, 1980; *Gorney et al.*, 1981; *Lundin et al.*, 1982; *Collin et al.*, 1984; *Yau et al.*, 1984, 1985; *Lennartsson and Shelley*, 1986]. In fact, it has recently been argued [*Chappell et al.*, 1987] that ionospheric plasma may fully populate the magnetosphere, with no significant solar wind source being required to account for observed magnetospheric charged particle populations. Recognition of the importance of the ionosphere as a source of magnetospheric plasma began with observations of heavy ions, previously believed to be gravitationally bound to low geocentric altitudes, at magnetospheric altitudes. As such observations continued to be reported, in diverse magnetospheric regions such as the ring current [*Johnson et al.*, 1977], the plasma sheet [*Peterson et al.*, 1981], and the plasma sheet boundary layer and tail lobes [*Eastman et al.*, 1984], it became apparent that escaping plasma transport from very low altitudes must be quite common. At the beginning of the 1980s, however, the questions of transport mechanisms and specific source regions were only beginning to be observationally addressed.

Observations of outflowing ionospheric ions have been reported by a number of authors in the last decade. Outflowing ion distributions which have apparently evolved, beginning with transverse (to **B**) acceleration and followed by magnetic mirror folding, have been observed near 1 R_E [*Sharp et al.*, 1977] in the topside ionosphere [*Klumpar*, 1979] and at sounding rocket altitudes [*Whalen et al.*, 1978; *Yau et al.*, 1983; *Moore et al.*, 1986*a*; *Kintner et al.*, 1989]. Since the launch of Dynamics Explorer 1 (DE 1), observation of low-energy ionospheric plasma outflows has become very common. The realization that the dayside magnetospheric cleft region represents a significant source of outflowing plasma began early in the DE mission, based on backward trajectory analysis of upflowing beams observed in high-altitude (2–4 R_E) polar cap field lines [*Waite et al.*, 1985]. This realization reached maturity with the work of *Lockwood et al.* [1985] who used DE 1 retarding ion mass spectrometer (RIMS) data to study the statistical occurrence of various types of ionospheric outflows. That work identified a persistent (occurrence probability exceeds 0.5 in source region) source of plasma emanating from the dayside auroral zone, showed that this source apparently favors the prenoon region of magnetic local time, and showed that there is a strong relationship between the low-latitude edge of the source region and the location of (usually downward) field-aligned currents. They labeled the observation of the distinctive RIMS spin-time signature associated with this outflow as an upwelling ion event (UWI). *Moore et al.* [1986*b*] and *Waite et al.* [1986] presented case studies of an UWI, observed near 1930 UT on day 71 of 1982. They derived bulk flow parameters for several species and demonstrated that the upwelling ion plasma core is hot and conically shaped, having undergone transverse energization at some lower altitude. They also noted a strong shear in the transverse electric field associated with the event.

The purpose of the present study is to more broadly investigate the bulk properties of UWIs, using RIMS and plasma wave instrument (PWI) quasi-static electric field data. The results of the study yield quantification of the densities and the upward field-aligned velocities and fluxes, for the ion species H^+, He^+, O^+, and O^{++}, associated with these flows. These parameters, as measured near the lower-latitude edge of the events, where the flows are most intense, will be presented. All of the available altitude normalized ion flux measurements from within the upwelling ion events are combined with the statistical occurrence probabilities derived by *Lockwood et al.* [1985] to produce spatial source strength distributions. Integration over these distributions yields an improved measure of the total low-energy ion outflow rate from this source region.

[1]NASA Marshall Space Flight Center, Alabama.
[2]Southwest Research Institute, San Antonio, Texas.
[3]Department of Physics and Astronomy, University of Iowa, Iowa City.

Paper number 90JA01095.
0148-0227/90/90JA-01095$05.00

2. INSTRUMENTATION

2.1. *The Spacecraft*

The observations presented in this report were gathered using instruments flown aboard the Dynamics Explorer 1 (DE 1) spacecraft. DE 1 was launched on August 3, 1981, into a highly elliptical polar orbit with apogee and perigee altitudes at 23,300 km (4.66 R_E, geocentric) and 570 km, respectively. The orientation of the orbit plane is fixed in the geocentric equatorial inertial (GEI) frame of reference, so that in the geocentric solar ecliptic (GSE) frame of reference, it is seen to rotate westward at a rate of 0.98°/day. This provides for approximately one full 360° rotation of the orbit plane in geocentric local time per year. Further, the DE 1 line of orbital apsides rotates about the negative orbit plane normal at a rate of 120°/year, so that the geographic latitudes of apogee and perigee drift retrograde at that rate. The spacecraft orbit, then, very nearly repeats itself, in the Earth's frame of reference, once every 3 years. These aspects of the spacecraft orbit influence our ability to study UWIs, not only because the source region has a limited geocentric solid angular extent, but also because the flowing plasma seems to evolve substantially with altitude. Therefore, the plasma characteristics which give rise to the distinctive RIMS UWI signature appear to exist only in a small region of space sampled by the spacecraft for several months once every 3 years. Furthermore, the orbit forces a phase-locked altitude-local time sampling which may bias the occurrence statistics of the local time extent of the upwelling ion source region. Other aspects of the DE mission have been described elsewhere [*Hoffmann and Schmerling*, 1981].

2.2 *Retarding Ion Mass Spectrometer*

Positive ion parameters presented in this report were obtained using the DE 1 retarding ion mass spectrometer (RIMS) [*Chappell et al.*, 1981]. The RIMS instrument consists of three similar sensor heads, one each viewing parallel and antiparallel to the spacecraft spin axis (negative and positive Z heads, respectively) and the third viewing in the spin plane (radial head). The two Z heads feature circular fields of view with half angles of 45°, while the radial head views a field which has a 45° half angle in the plane perpendicular to the spin plane and a 20° half angle in the spin plane. Since the DE 1 spin axis is nearly perpendicular to the geomagnetic field, the fields of view of the two Z heads are centered nearly perpendicular to that field, and the field of view of the radial head sweeps through a nearly full range of pitch angles with the spacecraft spin. All three sensor heads were designed to discriminate among incoming positive ions on the basis of energy per charge (0–50 eV/q), using a retarding potential analyzer (RPA), and on the basis of mass per charge (1–32 amu/q), using a magnetic mass spectrometer. Further, each sensor utilizes two detectors that are sensitive to ions with mass ratios of 4 to 1 such that, for example, while one detector is viewing O^+, the other is viewing He^+. The RPA on the radial head failed in late 1981, with the retarding grid having become electrically grounded to the spacecraft chassis so that, subsequent to the failure date, all ions with energies per charge greater than any positive spacecraft potential were passed into the magnetic mass spectrometer. The mass spectrometer, in turn, is characterized by a finite energy passband, whose width is dependent upon the species mass per charge and varies from approximately 250 eV for H^+ down to 16 eV for O^+. The upwelling ion densities, field-aligned bulk velocities, and fluxes presented below were derived using ion data from the RIMS radial head.

2.3. *Quasi-Static Electric Fields*

Quasi-static electric field data presented in this report and used in deriving ion bulk parameters were obtained using the Z axis antenna of the plasma wave and quasi-static electric field instruments [*Shawhan et al.*, 1981]. This tubular, 9-m (tip to tip) antenna is sensitive to the electric field component perpendicular to the spacecraft spin plane. The geomagnetic field is nearly (within 5° in 95% of our cases and always within 12° for our data set) contained within the DE 1 spin plane, so that the Z component electric field is associated with convective plasma drifts which are approximately within the spin plane and perpendicular to the ambient geomagnetic field. This electric field component is provided at a rate of 16 samples s^{-1} over a nominal range of 0.5 mV m^{-1} to 2 V m^{-1}. Characteristics of this instrument which are pertinent to the analysis techniques employed in this study will be described below.

3. DATA ANALYSIS

3.1. *Data Selection*

The observations presented here are taken from a subset of upwelling ion events identified by M. Lockwood through a survey of the RIMS data as displayed in the DE 1 microfiche (with format similar to Figure 2*a* displaying data for the species H^+ and He^+) in conjunction with his study of the occurrence of various types of terrestrial ion outflows [*Lockwood et al.*, 1985]. Lockwood et al. used a qualitative visual signature identification technique to identify these upwelling ion events. The RIMS spin-time upwelling ion event signature has been described elsewhere (see, for example, Plate 3 of *Lockwood et al.* [1985]). This signature is again illustrated in the O^+ data presented in Figure 2*a*, where the count rate in the O^+ channel is shown plotted in grey scale versus UT (along with certain orbital parameters) along the abscissa and the RIMS radial head viewing direction, with respect to the spacecraft ram direction, along the ordinate. The solid and dashed lines running through the spectrogram from left to right indicate viewing angles along the positive and negative geomagnetic field directions, respectively. For northern hemisphere passes, ions detected while viewing along the positive magnetic field direction are moving in the antifield direction and, therefore, away from the Earth. The signature of the event is evident in Figure 2, beginning near 2320 UT and continuing until just past 2327 UT. The ramp-like upward flux intensification, followed by a sharp cutoff and return to ram-dominated flow into the instrument at the low-latitude edge of the event, typifies the signature of these events used by Lockwood et al. in their fiche survey.

Having surveyed the available data obtained between October 1981 and October 1983, Lockwood et al. identified 86 upwelling ion events. These events were identifiable in the fiche for periods of time ranging from 1 to 15 min, providing a total of nearly 450 min of observation within the events. Of these 86 events, we have selected 39 for inclusion in the analysis for this report. This selection was based, in part, on the requirement that the RIMS instrument be operating in a mode without aperture bias applied to the instrument entrance and on the further requirement that the measured Z component of the electric field was deemed reliable. The RIMS instrument features an aperture bias capability, whereby a negative electrostatic potential may be applied to a grid at the entrance aperture, in order to overcome the effects of a positive spacecraft potential, allowing access of very low-energy ions to the instrument. Of the 86 upwelling ion events identified in the Lockwood et al. study, 20 were from times when RIMS was

operating in the aperture bias mode, and analysis of these events has been deferred pending the development of routine analysis tools for this mode. For another 8 events, either the digital RIMS data or the attitude and orbit data were unavailable. Of the remaining 58 events, 16 were rejected because the Z antenna dc electric field data were deemed unreliable. This antenna has a length of 9 m tip to tip, as compared with the spin plane antenna which is 200 m long. It is known to be subject to stray fields that originate from differential spacecraft charging and can have large amplitude relative to the fields of interest. This left 42 events, from which 2 were rejected due to a combination of no electric field data available and highly variable, difficult to interpret ion data and 1 was rejected due to the apparent presence of a telemetry dropout during the event. Thus, 39 of the original 86 events, or 45%, have been processed to obtain ion bulk parameters along the spacecraft track. Of these, 5 have no electric field data, and values of $E_z = 0$ have been assumed. These 39 events, consisting of a total of nearly 200 min of observation, constitute the data set used in the present analysis.

3.2. *Derivation of Ion Bulk Parameters*

Due to the failure of the RIMS radial head RPA, ion energy spectra are not available in the spin plane data. This situation has led to the development of an alternative technique for deriving ion bulk parameters from the RIMS radial heat data. This geometrical technique, developed by *Chandler and Chappell* [1986], provides a measure of the field-aligned ion bulk velocity and field-aligned ion flux of all ions of a given species which fall within the energy passband of the magnetic mass spectrometer. Derivation of the field-aligned bulk velocity depends upon the presumption that there are three distinct contributors to the species bulk velocity in the spacecraft spin plane and frame of reference (see Figure 1). These contributors are the spacecraft-induced ram velocity ($\mathbf{V}_r$), **E x B** drift ($\mathbf{V}_{ExB}$) and field-aligned drift ($\mathbf{V}_\parallel$) velocities. The spacecraft ram component is obtained from the orbit and attitude data base, while the **E x B** drift component is derived, using measured electric and magnetic fields, as

$$\mathbf{V}_{ExB} = \frac{c\mathbf{E} \times \mathbf{B}}{|\mathbf{B}|^2} \approx 10^{-2} \frac{E_z}{|\mathbf{B}|} \hat{(y)} \quad \frac{\text{km}}{\text{s}} \tag{1}$$

where, on the extreme right-hand side, E_z is the measured Z component of the electric field, expressed in mV m^{-1}, and **B** is expressed in gauss. Here, we have used the approximation that the magnetic field lies in the spin plane of the DE 1 spacecraft. As was mentioned above, this approximation is always good to within 12° for the data used in this study. Then, the total spin plane ion species bulk velocity in the spacecraft frame of reference is given as

$$\mathbf{v}_{\text{spin plane}} = (v_{rx} + v_\parallel)\,\hat{\mathbf{x}} + (v_{ry} + v_{ExB})\,\hat{\mathbf{y}} \tag{2}$$

where $v_\parallel$ is the field-aligned bulk velocity we are trying to determine, v_{rx} and v_{ry} are the X and Y components of the ion ram velocity, and

$$\hat{\mathbf{x}} = \hat{\mathbf{B}} \qquad \hat{\mathbf{y}} = \hat{\mathbf{z}} \times \hat{\mathbf{x}} \qquad \hat{\mathbf{z}} = -\hat{\omega}_{sc} \tag{3}$$

Note that positive values of field-aligned bulk velocity correspond to upward and downward drifts in the southern and northern hemispheres, respectively. All field-aligned drifts presented in this paper are upward, however, and we have plotted these as positive. Here, $\hat{\omega}_{sc}$ is parallel to the DE 1 spin angular momentum. The unknown parallel drift velocity is given as

$$v_\parallel = (v_{ry} + v_{ExB})\cot(\alpha) - v_{rx} \tag{4}$$

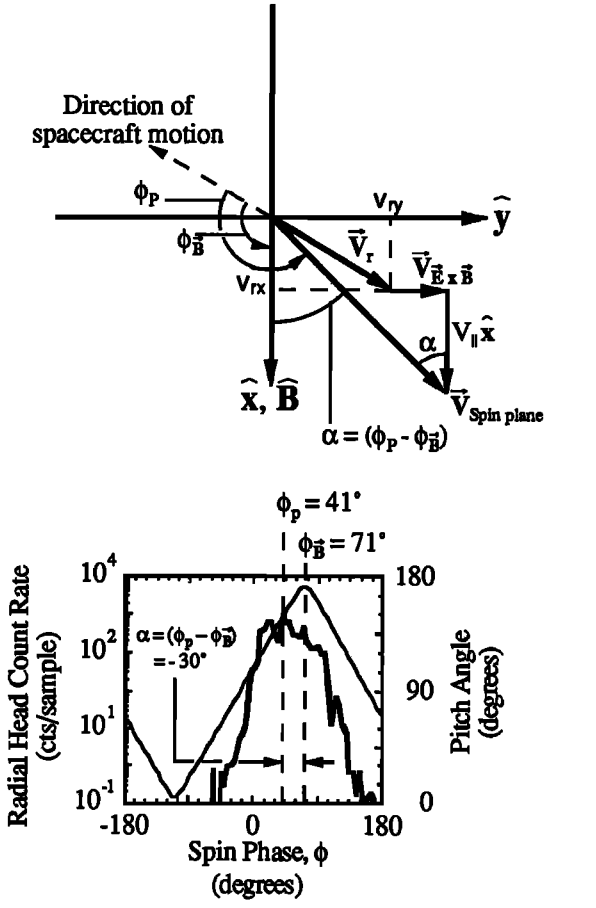

Fig. 1. The coordinate system and geometry used for computing ion species upward bulk velocity from RIMS spin curves and PWI electric field data is displayed in the top panel. At the bottom, a typical RIMS count rate spin curve is shown, and the meaning of angles identified in the sketch above is illustrated. The magnetic pitch angle at which counts are accumulated is displayed as the triangular wave in the bottom panel.

The angle α is measured as the difference

$$\alpha = \phi_p - \phi_B \tag{5}$$

in spin phase angles between the location (ϕ_p) of the centroid of the distribution of ion counts with spin phase and the direction (ϕ_B) along which the positive magnetic field direction is viewed. Spin phase angle (ϕ) is that measured about $+\mathbf{z}$, from the spacecraft velocity vector to the RIMS radial head look direction. In order to derive the field-aligned ion flux for a given species, the product of the instrument count rate and calibrated instrument sensitivity factors are cosine weighted, with respect to the spin plane velocity vector (given in equation (2), above), and integrated over spin phase angles, yielding the flux (J_T) along the direction of the total spin plane velocity vector. The field-aligned flux is then obtained as the product

$$J_\parallel = J_T \cdot \frac{v_\parallel}{|\mathbf{v}_{\text{spin plane}}|} \tag{6}$$

and the species particle density is estimated as

$$n \approx \frac{J_T}{|\mathbf{v}_{\text{spin plane}}|} = \frac{J_\parallel}{v_\parallel} \tag{7}$$

where $|\mathbf{v}_{\text{spin plane}}|$ is determined using equation (2), having deter-

mined $\mathbf{v}_{ExB}$ using measured fields as in equation (1), the ram components using orbit and attitude data in conjunction with magnetic field data, and $v_\parallel$ using equation (4) as described above. Our estimate for the species particle density is actually a lower bound, which disregards the possible presence of ions at energies lower than any positive spacecraft potential. This technique has been applied to data obtained in and near the 39 upwelling ion event intervals included in this study. We have used 1-min data averages throughout in analyzing the PWI electric field and the RIMS ion data.

3.3. *Error Analysis*

The above analysis involves two potential sources of error. First, for angles (α) near π or 0, corresponding to highly field-aligned or anti-field-aligned flows, the analysis produces values of $v_\parallel$ which are unrealistically large and positive or negative, respectively, for any nonzero difference $(v_{ry} - |v_{ExB}|)$. We have discarded results which yield a total velocity so large that the corresponding ion kinetic energy per charge would be too large to be passed by the magnetic mass spectrometer. The accuracy with which we can determine α is on the order of $\pm 2°$, so that the analysis of flows which are in actuality within $\sim 2°$ of being field-aligned would be expected to produce values of $v_\parallel$ whose magnitudes are arbitrarily large. We have propagated an uncertainty of $\pm 2°$ in α through the analysis.

Second, the accuracy with which we know the values of the Z component of the dc electric field is limited by the performance of the PWI Z antenna in these low- to medium-density plasma regimes. We have carefully examined the electric field data on a case-by-case basis and selected only those events characterized by spin-averaged field profiles which vary smoothly, or with reasonably small amplitude, both immediately prior to and following the upwelling event itself, as identified in the ion data. Further, we have derived estimates of the magnitude of the uncertainty in the values of E_z, in the manner described below, and propagated these through the analysis. In processing the electric field data, we have begun by producing 4-s (spacecraft spin period = 6 s) averages ($E_{z,4\ s}$) and standard deviations ($\sigma_{4\ s}$) about the means of the 16 sample s^{-1} data, producing 15 pairs of values per minute. The mean values of these two quantities represent 1-min averages of E_z, which we have used in the computation of ion bulk parameters, and of $\sigma_{4\ s}$, which represents a spin period time scale error estimate. Further, a 1-min time scale error estimate ($\sigma_{60\ s}$) is derived as the standard deviation of the 15 values of $E_{z,4\ s}$ about their mean. These two error estimates, in addition to a nominal uncertainty of 4 mV m^{-1}, have been treated as independent contributors to the uncertainty in E_z, as

$$\Delta E_z = \sqrt{\sigma_{4\ s}^2 + \sigma_{60\ s}^2 + \left(4\ \frac{\text{mV}}{\text{m}}\right)^2} \tag{8}$$

4. RESULTS

4.1. *Results for a Single Pass*

Figure 2 illustrates the nature of the data used in the analysis and the results for a single pass on day 60 of 1982. These results are not typical, in that this was a particularly intense event, observed at unusually low altitude on a day characterized by a sustained high level of geomagnetic activity. The ion and electric field data shown in Figure 2 are plotted against UT, with various spacecraft orbital parameters also indicated along the horizontal axis. The interval selected shows a DE 1 pass from the northern polar cap across the dayside auroral zone.

Figure 2*a* shows the RIMS radial head spin time spectrogram for O^+ and has been described above in the context of data selection. The full time resolution Z component electric field data and the processed Z component data are shown in Figure 2*b* and Figure 2*c*, respectively. The full time resolution electric field data in Figure 2*b* show not only the steady offset induced by spacecraft motion across the magnetic field, but also a distinct modulation induced by nonstationary spacecraft sheath structure. Recall that since the electric Z antenna is aligned with the spacecraft spin axis, spin modulation in this signal is not expected in the presence of spacecraft sheath structure unless the structure changes with spin phase. Note the large-amplitude, unresolved excursions in the electric field signature near 2327 UT. The long wire electric antenna on DE 1 shows a similar signature, which is quite common near the UWI source region. The possible role of these large-amplitude and highly structured electric fields in producing the upwelling ion flows will be addressed in a future publication. The final electric field data product, which is used in computing the ion bulk parameters, is shown in Figure 2*c*, where values of ΔE_z as given in equation (8) are used in determining the size of the error bars. In these 1-min averages, the contribution induced by spacecraft motion has been explicitly removed, and the spin modulation removed by the averaging procedure. It is evident from a comparison of Figures 2*b* and 2*c* that significant structure, present in the unprocessed field data, is lost in the 1-min data product.

In Figures 2*d* through 2*f* the bulk parameters ($V_\parallel$, $J_\parallel$, and n, respectively), derived as described above, are presented for each of the ion species H^+, He^+, O^+, and O^{++}. Although the field-aligned ion velocities and fluxes are generally upward throughout the interval, they are most pronounced during the minute extending from 2325:30 UT to 2326:30 UT. It is at this time that the event is said to maximize in intensity and that the spacecraft is thought to be directly downstream of the upwelling ion flow source, in the dayside polar cleft.

4.2. *Typical Flux, Velocity, and Density Levels at Event Maxima*

The ramplike upwelling ion signatures observed as the spacecraft passes from high latitudes through the dayside auroral zone, followed by sharp cutoffs at the low-latitude edge, are common features of UWI signatures. These features are interpreted in terms of a convective effect, whereby the source of the ion upwelling exists in a localized zone near the low-latitude edge of the event and ions are convected to higher latitudes, dispersing them poleward of the source. From this point of view, the region where the upward flux maximizes, near the low-latitude edge of the event, may be considered to be most closely associated with the source region. The ions observed in this region are characterized by the shortest flight paths from source to observer and, as we note, are those with the largest upward field-aligned velocities, slower particles having been convected further poleward by the time they reach the spacecraft altitude. We have therefore taken the ion bulk parameters measured at this location to be indicative of the intensity of a given event, with the proviso that there is a bias toward larger field-aligned velocities.

Having selected the analyzed data for 39 events, we have isolated the ion bulk parameters at the time in each event when the maximum flux was observed. Figure 3 shows a scatter plot of the measured maximum flux versus the inferred density for each of the four species: H^+, He^+, O^+, and O^{++}. Points lying along the two lines running through the plot represent upward bulk velocities of 1 km s^{-1} and 10 km s^{-1}. While the measured fluxes

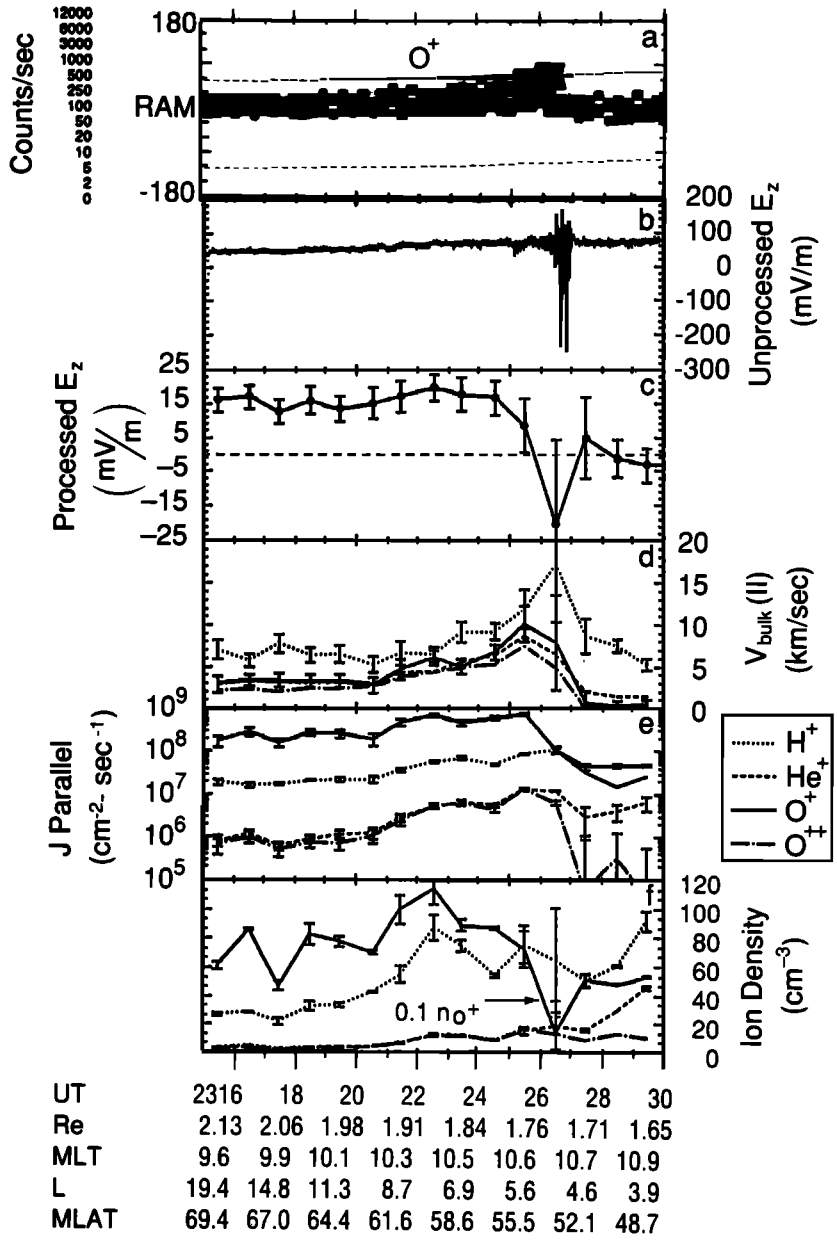

Fig. 2. RIMS ion data and PWI electric field data are displayed as functions of time for a dayside auroral zone pass on day 60 of 1982. The top panel shows a RIMS O^+ spin-time count rate spectrogram in standard RIMS format. The second and third panels from the top show PWI dc electric field data in almost raw and processed formats, respectively (see text). The bottom three panels display derived ion species bulk parameters of upward velocity, upward flux, and particle density for several ion species. Note that the O^+ ion densities have been divided by 10. Various orbital parameters, as well as UT, are listed along the abscissa.

and densities vary over several orders of magnitude, the upward velocities tend to lie between 1 and 10 km s^{-1} for the heavier species and near or above 10 km s^{-1} for the lighter species. Plots of the relative occurrence frequency of maximum density, field-aligned velocity, and flux observed in these events for the species H^+, He^+, O^+, and O^{++} are presented in Figures 4*a* through 4*c*, respectively. In the case of the maximum flux (Figure 4*c*), the flux values plotted along the abscissa have been mapped to a common altitude of 1000 km, according to an r^{-3} scaling law, while the densities and velocities are plotted as measured, irrespective of spacecraft altitude. This is in contrast to the flux values plotted in Figure 3, which are as measured, irrespective of altitude. In Figure 4, the species are differentiated by the plotting symbols used.

Figure 4*a* shows that these events are typically oxygen-rich near the source region with typical fractional and absolute O^+ ion densities of 0.9 and 1000 ions cm^{-3}, respectively. This represents somewhat large O^+ densities for these altitudes (~1.5–2 R_E) as compared with polar cap field lines (see, for example, the total electron density results of *Persoon et al.* [1983], or the ion species density results of M. O. Chandler et al. (Observations of polar ion outflows, submitted to *Journal of Geophysical Research*, 1989). Such large O^+ densities are indicative of increased ionospheric scale heights, probably associated

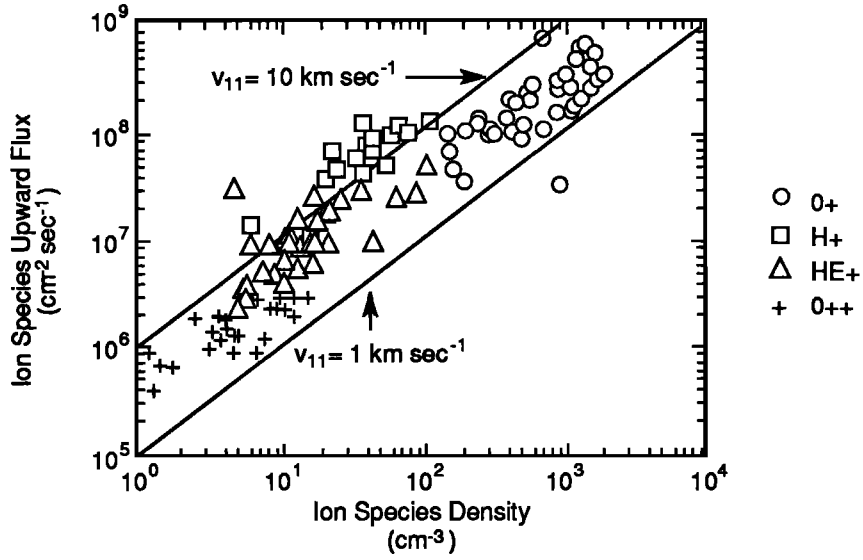

Fig. 3. A scatter plot of measured upward ion flux versus measured ion density at the low-latitude edge of UWIs is shown for several ion species. The data were gathered over a range of DE 1 altitudes between 1.3 and 2.1 R_E. The straight lines running through the plots show the loci of points for ions moving upward at 1 km s^{-1} (lower line) and 10 km s^{-1} (upper line).

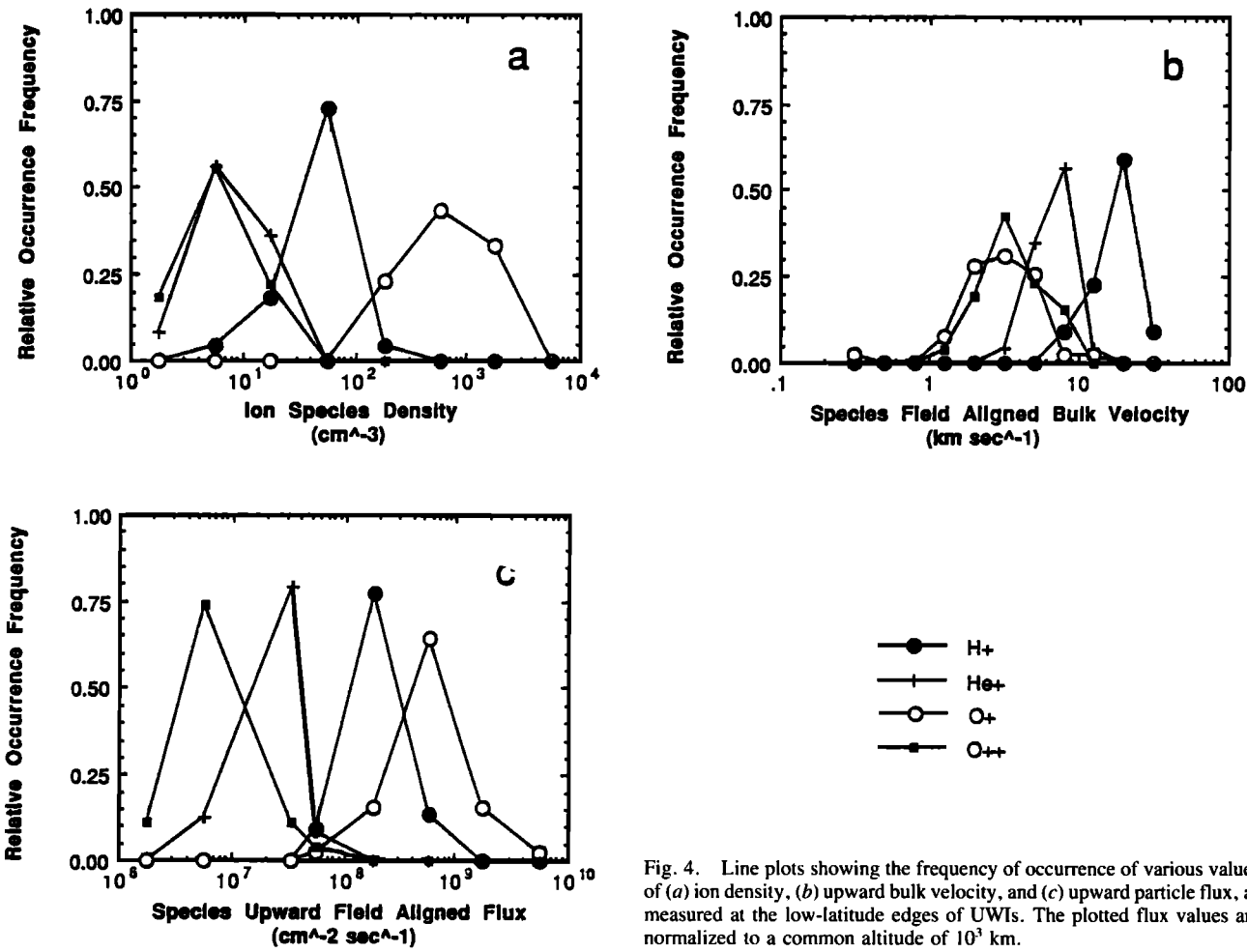

Fig. 4. Line plots showing the frequency of occurrence of various values of (*a*) ion density, (*b*) upward bulk velocity, and (*c*) upward particle flux, as measured at the low-latitude edges of UWIs. The plotted flux values are normalized to a common altitude of 10^3 km.

with bulk ionospheric heating at much lower altitudes. These O^+ density results are consistent with the model polar wind results of *Schunk and Sojka* [1989]. Our H^+ density results are in wide variance with those of Schunk and Sojka, however, with typical observed H^+ densities of <100 ions cm^{-3} at geocentric distances between 1.5 and 2 R_E as compared with model results in excess of several thousand ions per cubic centimeter (at 2500 km altitude).

The upwelling O^+ flux (Figure 4*c*) is also dominant over that associated with the other ions, with maximum scaled flux levels which typically approach 10^9 ions cm^{-2} s^{-1}, far in excess of predicted polar wind O^+ flux levels. On the other hand, the largest field-aligned velocities are measured in the H^+ ions, for which the upward bulk velocity is generally greater than 10 km s^{-1} near the latitude of the source region. More modest bulk velocities, of the order of 3 km s^{-1}, are typically observed in the O^+ ions.

We have found that the measured upward field-aligned bulk velocity varies systematically with species mass per charge, with light ions moving upward with higher velocity than the heavier ions. This point is illustrated with Figure 5, where characteristic upward bulk velocities are plotted as a function of species charge per unit mass. The distribution of velocities shown in Figure 5 is dominated by the H^+ ions (at $q/m = 1$) which are clearly moving upward much faster than the other species, although the He^+ ions are also significantly faster than the two species (O^+ and O^{++}) plotted. The trend is not as strongly supported when comparing the O^+ and O^{++} ions either in this figure, which is derived from the mean values of the bulk velocities observed at maximum flux, or on a case-by-case basis, where the O^+ is often seen to be moving upward with higher velocity than the O^{++}. We have shown a power law fit to the data in Figure 5, which yields

$$v_\parallel \cong 17 \left\{ \frac{Z}{(m/m_p)} \right\}^{0.6} \frac{\text{km}}{\text{s}}$$

where Z is the ion charge state and (m/m_p) is the ion mass, normalized to the proton mass. Processes yielding energies proportional to ion charge but independent of ion mass would give rise to a square root dependence of $v_\parallel$ upon (q/m). An example of such a process is acceleration in a parallel (to **B**) electric field. However, the warm and anisotropic nature of these upwelling plasmas, along with their high density, suggests that the outflow arises due to transverse heating in the topside of an already warm cleft ionosphere, followed by upward magnetic folding of the ion distributions. The analysis of the thermal properties of these events is beyond the scope of this report and will be reported in a future paper. However, it is to be noted that upwelling ion flows are typically warm and anisotropic, with temperatures (transverse to **B**) of several electron volts, as reported by *Moore et al.* [1986*b*].

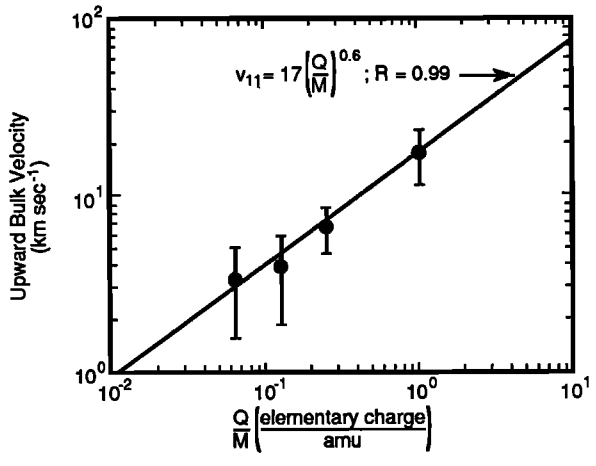

Fig. 5. Mean values of ion species upward bulk velocities are plotted versus the species charge per unit mass. The velocities plotted are those derived from measurements taken at the lower-latitude edges of UWIs, where the upward flux is seen to maximize. The line indicates a power law fit to the data, with the fit parameters indicated.

Delcourt et al. [1989] have modeled the evolution of these ion flows using particle ray tracing techniques in realistic gravitational, electric, and magnetic fields. They have found that the upwelling ions generally escape the Earth's immediate vicinity in large numbers and travel in an extended plume over the polar cap into the geomagnetic tail and plasma sheet, where the heavier species are rather dramatically accelerated as they cross the neutral sheet.

4.3. *Bulk Parameter Correlations and Dependence on Location and Geomagnetic Activity*

The relationship between spatial location and the occurrence of ion upwelling has been investigated by *Lockwood et al.* [1985]. Their study showed that for DE 1 altitudes below 3 R_E, geocentric, the probability of observing the asymmetric RIMS spin-time signature of an upwelling ion event peaks at near 0.7 in the prenoon magnetic local time (MLT) sector and at invariant latitudes (IL) between 75° and 80° (see their Plate 4*c*). The question arises as to whether the intensity of the upward flow shows systematic variation with the location of the source region. In Figure 6, we present scatter plots of the upwelling O^+ flux, measured during the minute of maximum intensity within the event and normalized to a common altitude of 1000 km, versus MLT (Figure 6*a*) and IL (Figure 6*b*). There is substantial scatter in the observations, with several particularly large flux values, and no apparent systematic trend. The intensity of the outflow does not seem to be correlated with the latitude or MLT at which the observations are made within the source region.

There is, however, some indication that the ion composition within these events varies systematically with magnetic local time, with the fractional minor species density increasing toward local noon. Figure 7 provides a convenient summary of the ion composition for a number of cases in which all four ion species were measured simultaneously. As noted earlier, the bulk of the ion plasma consists of O^+, comprising about 90% of the ion density, while H^+ contributes ~10%, and He^+ and O^{++} each contribute ~1%. The upwelling O^+ flux typically represents a smaller percentage (~70%) of the total upward flux, due primarily to the larger H^+ bulk velocities. In Figure 7, we show the fractional ion composition plotted versus the magnitude $|\text{MLT} - 12|$ to illustrate the existence of a possible systematic relationship between proximity to local noon and ion composition within these events. Note that values are plotted along the abscissa without regard to whether data were collected in the prenoon or postnoon sector. The fractional composition of the minor species appears to increase with proximity to local magnetic noon. The case for the compositional dependence upon MLT is stronger for O^{++} (linear correlation coefficient = –0.7) than for the other species. The reason for this dependence is unclear. The O^+ density (and therefore total ion density) appears to decrease with proximity to noon, although the data are scattered (linear correlation coefficient $|R| \sim 0.3$), while the absolute minor species densities show no significant trend. These apparent trends in the ion composition could be anomalous, resulting from correlations between MLT and altitude imposed by the DE 1 orbit. Further study of this subject will be required.

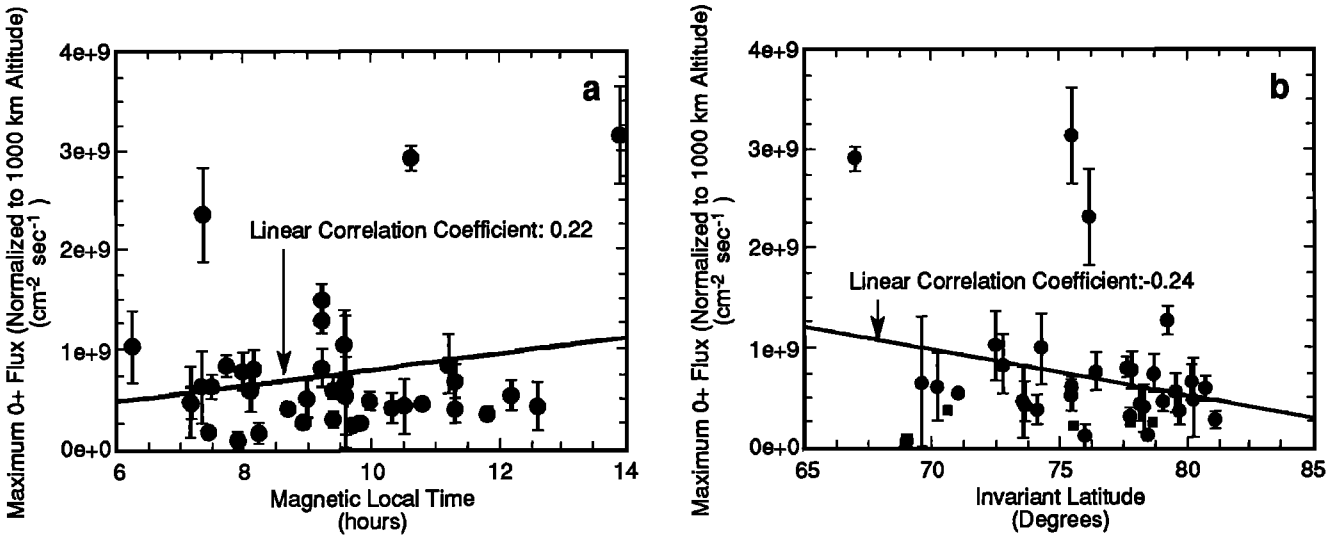

Fig. 6. Upward O^+ flux (normalized to 1000 km altitude) is plotted in scatter plots versus (*a*) the MLT and (*b*) the IL at which the observations were made. The flux shown is that measured at the low-latitude edge of UWIs, where the flux maximizes. Linear fits to the data and the associated linear correlation coefficients are shown.

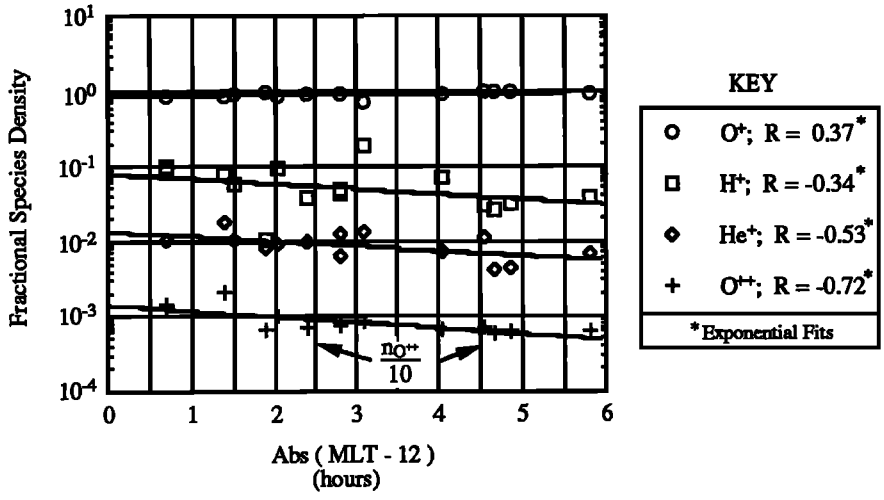

Fig. 7. The fractional densities of the species O^+ (open circles), H^+ (open squares), He^+ (open diamonds), and O^{++} (crosses) are displayed in scatter plot format versus the separation (in hours) from local magnetic noon at which the observations were made The data for O^{++} have been divided by 10 to provide for a clearer display. The composition data are as determined during the minute within a given UWI when the upward O^+ flux maximizes, generally at the lower-latitude edge of the event.

As shown by *Lockwood et al.* [1985], the invariant latitude of the upwelling ion source region varies systematically with geomagnetic activity, moving to lower latitudes with increasing values of the 3-hour *Kp* index. The association of this upwelling source region with the geomagnetic polar cleft and its systematic latitudinal variation is further illustrated in Figure 8, where the invariant latitude at which the maximum upwelling O^+ flux occurs is plotted versus a measure of the interplanetary magnetic field (IMF) B_z component. The values of B_z plotted were obtained from hourly averages published by the National Space Science Data Center (NSSDC) World Data Center A for Rockets and Satellites. These data are a compilation based on IMP 8 and ISEE 3 observations. The plotted values represent weighted (and corrected for solar wind transit time) hourly averages of B_z during the hour immediately preceding the minute in UT during which the flux observation was obtained. For example, in the case of day 71 of 1982 the maximum O^+ flux was observed at 1934 hours UT. The value of B_z associated with that event is taken as

$$\langle B_z \rangle = \frac{34[B_{z(1900\text{-}2000)}] + 26(B_{z(1800\text{-}1900)})}{60} \quad (9)$$

where $B_{z(xx00\text{-}yy00)}$ was obtained from the World Data Center data base. We have indicated a least squares linear fit to the data, which yields a correlation coefficient of 0.72. We have also shown (dashed lines) the linear least squares results of *Carbary and Meng* [1986], giving the fitted locations of the poleward and equatorward cusp boundaries, based on DMSP F-2 and F-4 low-energy electron signatures, as functions of B_z (measured by the

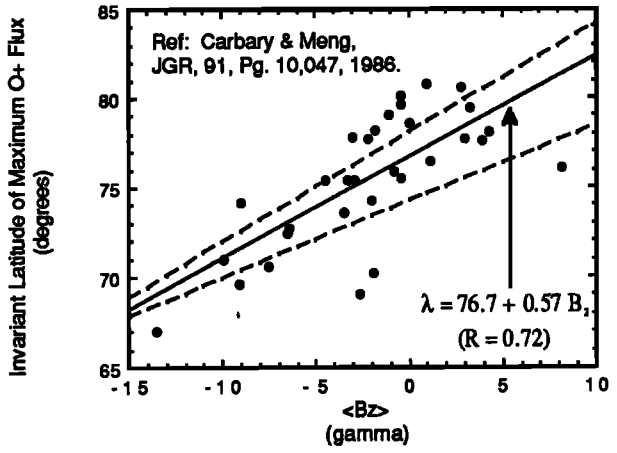

Fig. 8. A scatter plot of the latitude at which the upward O^+ flux maximizes within UWIs, versus the preceding hourly average of the IMF B_z component (corrected for solar wind transit time to the magnetopause). The solid line represents a linear least squares fit to the data. The two dashed lines show the locations of the upper- and lower-latitude edges of the cleftlike (see text) electron precipitation signatures as functions of B_z. These edges are as determined in the study of *Carbary and Meng* [1986].

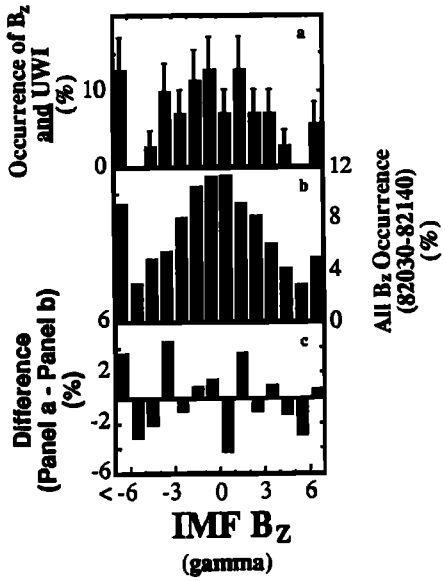

Fig. 9. The occurrence, during the period between days 36 and 268 of 1982, of various values of the IMF B_z component is studied, both in relationship with the occurrence of UWIs and independent of such occurrence. (*a*) The distribution of B_z values measured during the hour immediately preceding a RIMS UWI observation. (*b*) The distribution of B_z for all the available data, without regard to RIMS observations. (*c*) The difference between the data in Figures 9*a* and 9*b*. These differences should reveal any significant trend in the dependence of the occurrence of dayside ion upwelling upon B_z. All IMF data are corrected for solar wind transit time to the magnetopause.

IMP 8/GSFC (Goddard Space Flight Center) magnetometer). We note here that although *Carbary and Meng* [1986] use the word "cusp," the study they performed applies to a broader region (in MLT) which is more properly referred to as the "magnetospheric cleft" [*Carbary and Meng*, 1986, Figure 2; *Newell and Meng*, 1988]. The distinction is significant because the cusp, found within a region highly localized near noon MLT, as thought to connect to the dayside magnetopause, while the cleft, found within a broad region which stretches across the dayside, is associated with the low-latitude boundary layer. Although, as in the Carbary and Meng study, there is significant scatter in the data, Figure 8 unambiguously locates the upwelling ion source region within the magnetospheric polar cleft, as identified by the low-energy electron signature.

There does not, however, appear to exist a strong relationship between either the occurrence probability or intensity of upwelling ions and the averaged value of the IMF B_z during the hour immediately preceding the observation of ion upwelling in the RIMS data. In Figure 9, we study the occurrence of values of B_z as observed, both in conjunction with an UWI observation and regardless of UWI observation. All three panels in Figure 9 feature an abscissa which is composed of B_z values binned in 1 γ bins, from -6 γ to $+6$ γ, with the leftmost bin including all observations of B_z less than -6 γ and the rightmost bin those with B_z greater than or equal to $+6$ γ. There were a total of 70 observed UWI events for which the IMF data were available during both the present and previous hours, allowing the weighted average described in the previous paragraph to be performed. The value plotted along the ordinate of Figure 9*a* represents the percentage of those 70 events which were characterized by a weighted hourly average of B_z which fell within the given bin. The error bar is derived from the square root of the number of samples in the bin. For example, 9 ± 3 of the events were associated with a value of B_z of less than -6 γ, yielding $12.8 \pm 4.3\%$ of the 70 samples. In Figure 9*b* the occurrence of frequency of B_z values, for all available hourly IMF data during the same time period as in Figure 9*a* (days 36–268 of 1982), are plotted for comparison. The distribution in Figure 9*b* is peaked near $B_z = 0$ and falls off quite symmetrically to either side. The large occurrences in the extreme bins are a reflection of the larger bin size. Figure 9*c* displays the differences between the data in the above two panels, such that the plotted values are equal to those plotted in Figure 9*a*, less those plotted in Figure 9*b*. If the occurrence of UWI events were dependent upon B_z, we would expect to see that reflected most clearly in Figure 9*c*. If, for example, UWIs were more likely to occur for negative values of B_z, we would expect to see positive differences in Figure 9*c* for $B_z < 0$ and negative differences for $B_z > 0$. No such trend is evident, and we conclude from these data that UWI occurrence is not dependent upon the average value of B_z during the hour immediately preceding event observation.

A similar statement can be made regarding the dependence of upwelling O^+ intensity on the averaged B_z values, as illustrated using the scatter plot of Figure 10. Here we have plotted the maximum upwelling O^+ flux, normalized to 1000 km altitude, measured during a given event versus the hourly averaged value of B_z for the hour immediately preceding event observation. The linear correlation coefficient of –0.14 indicates no significant dependence among the parameters plotted. These results are somewhat surprising, in view of recent observations of *Lockwood et al.* [1988] which suggest that dayside ion upwelling may be a direct consequence of magnetic coupling at the subsolar magnetopause. Further study of the relationship of UWI events to interplanetary and magnetospheric conditions will be the subject of a future publication.

4.4. *Cleft Region Source Strength*

The upward ion flux levels discussed in the previous sections are not typical of the entire dayside auroral zone, but are representative of the most intense portions of the upwelling flows,

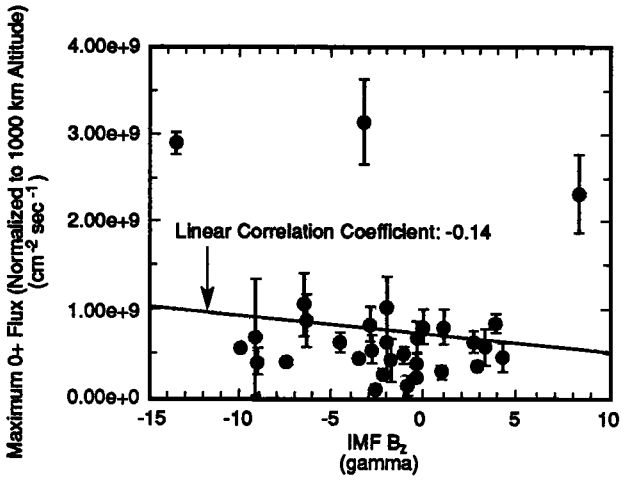

Fig. 10. Upwelling O^+ flux is displayed as a scatter plot versus the immediately preceding hourly averaged value of the IMF B_z component, corrected for solar wind transit time to the magnetopause. The flux values plotted are the maximum values measured within the UWIs and are normalized to a common altitude of 10^3 km. A linear fit to the data, as well as the resulting linear correlation coefficient, is indicated.

in the immediate vicinity of the source region. We have computed bulk parameters from regions downstream (generally poleward) of the source region as well. All the measured fluxes, as well as a measure of the occurrence frequency of dayside ion upwelling, need to be incorporated into any estimate of the total ion outflow from this ionospheric source. The expectation value for the upward particle flux at any location may be expressed as the product of the upward flux measured at that location at the time when an upwelling ion event is observed and the probability that an upwelling ion event will be observed at that location. We have binned our ion flux measurements in IL and MLT and combined them as a product with similarly binned values of the occurrence probabilities reported by *Lockwood et al.* [1985]. We have used 5° IL bins between 50° and 90° and 1-hour MLT bins from 0 to 24 hours. The mean flux in a given bin is taken as

$$\overline{J_{i,j}} = \frac{\sum_{n=1}^{N} J_{i,j,n}}{N} \tag{10}$$

where $J_{i,j,n}$ represents the nth of a total of N flux observations (normalized to 1000 km altitude) in the angular bin associated with the indices (i,j). The expectation value for the flux in the bin (i,j) is then given as

$$\langle J \rangle_{i,j} = (\overline{J_{i,j}}) \times (f^{u}_{i,j}) \tag{11}$$

where $f^{u}_{i,j}$ is the occurrence probability reported by *Lockwood et al.* [1985]. Expectation values computed in this manner are presented in Figure 11 for the species H^+, He^+, O^+, and O^{++}, where the value of $\log_{10}(\langle J \rangle_{i,j})$ is plotted in polar grey scale versus IL and MLT. The expectation values plotted in Figure 11 represent the closest estimate we can make at this time of the mean upwelling source strength for the various ion species shown. The outflowing source region may extend poleward of the region shown in Figure 11; however, such an extension is not identifiable within the context of the UWI signature identification on which this work is based. As in the case of the maximum event fluxes reported in previous sections, O^+ and H^+ show the most

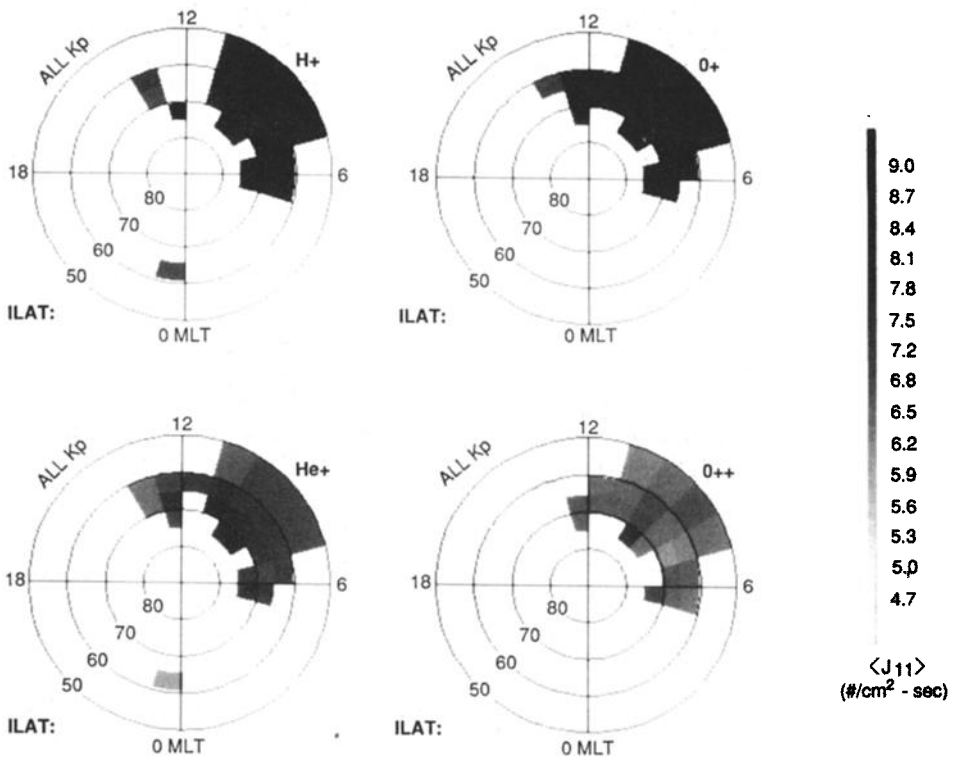

Fig. 11. The expectation value $\langle J_{\parallel} \rangle$ for the upward parallel flux is plotted for the ion species H^+, O^+, O^{++}, and He^+, in polar grey scale format versus IL and MLT. The flux in a given IL-MLT bin is derived as the product of the average flux measured in that bin within UWIs and the probability that an UWI will be observed within the bin.

intense outflows, followed by He^+ and O^{++}. In all cases, the source region is rather spatially structureless.

The fluxes shown in Figure 11 represent the ion flux expected at an altitude of 1000 km, having been scaled from the observation altitudes according to an $(r/r_0)^3$ dependence, where r and r_0 are the geocentric radii of the observation point and the 1000 km altitude surface, respectively. The total hemispheric particle outflow rate may be obtained by integrating over the distributions shown in Figure 11. To facilitate the integration, the fluxes are further scaled to the Earth's surface, where IL and the spherical magnetic latitude are equivalent. The total terrestrial outflow (I) from this dayside source region, for a given ion species, is then given as

$$I = 2\int_H \langle \mathbf{J}(r,\lambda,\phi)\rangle \, d\mathbf{a}$$

$$= 2R_E^2\left(\frac{r_0}{R_E}\right)^3 \int_0^{2\pi} d\phi \int_0^{\pi} d\lambda \, \langle J_\parallel(r_0,\lambda,\phi)\rangle \qquad (12)$$

where we have approximated the geomagnetic field lines as radial and the factor of 2 accounts for source regions in each hemisphere. This integration has been numerically carried out over the distributions of fluxes shown in Figure 11. The resulting outflows are listed in Table 1. These numbers may underestimate the total outflow, since significant UWI outflows may occur poleward of regions identified as being within UWIs.

TABLE 1. The Total Rate $\langle J_\parallel \rangle$ at Which Ions Flow out of the Dayside Cleft Region

Ion Species	$\langle J_\parallel \rangle$, ions s^{-1}
H^+	5×10^{24}
He^+	9×10^{23}
O^{++}	2×10^{23}
O^+	2×10^{25}

Flows from both hemispheres are included.

The ion outflow is dominated by O^+, with 2×10^{25} ions s^{-1} emanating from the dayside cleft region. The H^+ source strength represents ~20% of the total outflow, while the minor species (O^{++} and He^+) are at the several percent level or less. These results are to be compared with those of *Yau et al.* [1985] who studied major ion outflows at energies such that $10 \text{ V} \leq E/q \leq 17$ kV. They reported extensively on outflows at latitudes including the auroral zone and polar cap, distinguishing among flow levels on the basis of geomagnetic activity, MLT/IL regime, and solar cycle. Many of the results of *Yau et al.* [1985] are summarized in their Table 1. They found the total net auroral zone ion outflow to lie between 2×10^{25} and 4×10^{25} ions s^{-1} for H^+ and between 1×10^{25} and 8×10^{25} for O^+, depending on geomagnetic activity and solar cycle. In our Table 1, we show a total UWI O^+ outflow of 2×10^{25} ions s^{-1}. This is of the same order as that reported by Yau et al. during geomagnetically quiet times. On the other hand, our results show a total H^+ outflow of 5×10^{24} ions s^{-1}, a factor of 5 smaller than that reported by Yau et al. during geomagnetically quiet times. We believe these figures apply to ions with energies less than or of the order of 10 eV/q. This is based on both the published work of *Moore et al.* [1986*b*] and on other, unpublished work, which show typical ion thermal energies within these events of 5 − 10 eV/q. The flux levels in the current study are representative of a wide range of geomagnetic activity. The available data do not permit breaking down the global UWI outflow according to geomagnetic activity. It appears, especially in the case of the O^+, that the UWI source represents a substantial fraction of the total global ion outflow.

5. CONCLUSIONS

With the data presented in the sections above we have reported the bulk properties of the upwelling ion plasma in the dayside cleft region. We have quantified the distribution of ion species density, upward bulk velocity, and flux within the cleft source region. Additionally, we have combined the bulk flow results from a number of these events with the occurrence probabilities obtained by *Lockwood et al.* [1985] to give reliable estimates of the source strength distribution as a function of MLT and IL. Finally, we have presented a measure of the total cleft region source strength in terms of the number of ions per second to flow away from the ionosphere. The following specific conclusions may be drawn from the work presented above.

1. All observed ion species are seen to participate in the ion upwelling. Within a given event, the upward flux typically maximizes near the low-latitude edge of the outflow. At that location, typical ion species densities, upward field-aligned bulk velocities, and upward field-aligned fluxes (mapped to a common altitude of 1000 km) are summarized in Table 2. The distributions about these typical values have been presented in Figure 4.

TABLE 2. Typical Ion Bulk Parameters as Measured Within, but Near the Lower-Latitude Edge of Upwelling Ion Events

Species Bulk Parameter	O^+	H^+	He^+	O^{++}
n, cm^{-3}	600	50	15	7
$v_\parallel$, km s^{-1}	3	16	7	4
$J_\parallel$,* particles cm^{-2} s^{-1}	6×10^8	2×10^8	10^7	6×10^6

*Scaled to a common altitude of 1000 km.

2. There is a systematic dependence of the upward field-aligned ion bulk velocity upon the species charge-to-mass ratio, with the velocity increasing approximately with the square root of q/m. This dependence is illustrated in Figure 5.

3. The intensity of UWIs, as measured by the maximum upward O^+ flux observed within an event, does not show significant systematic variation as a function of MLT or IL. This is indicative of a rather uniform outflow from the dayside cleft region. This point is illustrated in Figure 6, where scatter plots of the maximum normalized O^+ flux versus MLT and IL are presented. The point is further illustrated, with respect to all measured flux values for the species H^+, He^+, O^+, and O^{++}, in Figure 11, where the expectation value of the normalized upward flux is shown plotted in polar form.

4. The ion density composition of the outflow shows a weak dependence upon MLT, however, with minor species, particularly O^{++}, representing a larger fractional composition near magnetic local noon. This point is illustrated in Figure 7.

5. The statistical association of UWIs with the dayside magnetospheric cleft, as identified by low-energy electron signatures [*Carbary and Meng*, 1986], is illustrated in Figure 8. This association points up the likelihood of a relationship between the phenomenon of dayside ion upwelling and the solar wind-magnetosphere interaction.

6. There is, however, no clear-cut relationship between either the occurrence or intensity of UWIs and the immediately preceding hourly averaged value of the IMF B_z component. These facts are illustrated in Figures 9 and 10, respectively. As the simplest

measure of the degree of electromagnetic coupling between the magnetosphere and solar wind, one might expect to find increased occurrence or intensity of UWIs with increasingly negative B_z if, for example, UWIs were directly associated with variable aspects of the large-scale auroral convection morphology or with the occurrence of magnetopause flux transfer events, both of which depend upon B_z. The results presented here indicate that neither is the case.

7. Our estimate of the ion outflow rates (including both hemispheres) from this dayside cleft source have been presented in Table 1. These estimates are given based on data collected between days 36 and 137 of 1982, and almost all were from northern hemisphere passes. Thus, they are generally representative of spring conditions during an active portion of the solar cycle. Virtually all levels of geomagnetic activity are represented. In the case of O^+ and H^+, these numbers validate the cleft ion fountain contributions used by *Chappell et al.* [1987] and *Delcourt et al.* [1989] in demonstrating the significance of the ionosphere as a magnetospheric plasma source.

Acknowledgments. The authors are grateful to the RIMS team at Marshall Space Flight Center (MSFC) and the programming staff of Boeing Corporation for assistance with the data reduction software. We would also like to thank the National Space Science Data Center (NSSDC) for providing the interplanetary magnetic field data. Support for C. J. Pollock came from the National Research Council, under their Resident Research Associateship program.

The Editor thanks M. Lockwood and A. W. Yau for their assistance in evaluating this paper.

REFERENCES

Balsiger, H., P. Eberhardt, J. Geiss, and D. T. Young, Magnetic storm injection of 0.9- to 16-keV/*e* solar and terrestrial ions into the high-altitude magnetosphere, *J. Geophys. Res.*, *85*, 1645–1662, 1980.

Carbary, J. F., and C. I. Meng, Correlation of cusp latitude with B_z and *AE* (12) using nearly one year's data, *J. Geophys. Res.*, *91*, 10,047–10,054, 1986.

Chandler, M. O., and C. R. Chappell, Observations of the flow of H^- and He^- along magnetic field lines in the plasmasphere, *J. Geophys. Res.*, *91*, 8847–8860, 1986.

Chappell, C. R., S. A. Fields, C. R. Baugher, J. H. Hoffman, W. B. Hanson, W. W. Wright, and H. D. Hammack, The retarding ion mass spectrometer on Dynamics Explorer A, *Space Sci. Instrum.*, *5*, 477–491, 1981.

Chappell, C. R., T. E. Moore, and J. H. Waite, Jr., The ionosphere as a fully adequate source of plasma for the Earth's magnetosphere, *J. Geophys. Res.*, *92*, 5896–5910, 1987.

Collin, H. L., R. D. Sharp, and E. G. Shelley, The magnitude and composition of the outflow of energetic ions from the ionosphere, *J. Geophys. Res.*, *89*, 2185–2194, 1984.

Delcourt, D. C., C. R. Chappell, T. E. Moore, and J. H. Waite, Jr., A three-dimensional numerical model of ionospheric plasma in the magnetosphere, *J. Geophys. Res.*, *94*, 11,893–11,920, 1989.

Eastman, T. E., L. A. Frank, W. K. Peterson, and W. Lennartsson, The plasma sheet boundary layer, *J. Geophys. Res.*, *89*, 1553–1572, 1984.

Ghielmetti, A. G., R. G. Johnson, R. D. Sharp, and E. G. Shelley, The latitudinal, diurnal, and altitudinal distributions of upward flowing energetic ions of ionospheric origin, *Geophys. Res. Lett.*, *5*, 59–62, 1978.

Gorney, D. J., A. Clarke, D. Croley, J. Fennell, J. Luhmann, and P. Mizera, The distribution of ion beams and conics below 8000 km, *J. Geophys. Res.*, *86*, 83–89, 1981.

Hoffman, R. A., and E. R. Schmerling, Dynamics Explorer program: An overview, *Space Sci. Instrum.*, *5*, 345–348, 1981.

Johnson, R. G., Energetic ion composition in the Earth's magnetosphere, *Rev. Geophys.*, *17*, 696–705, 1979.

Johnson, R. G., R. D. Sharp, and E. G. Shelley, Observations of ions of ionospheric origin in the storm-time ring current, *Geophys. Res. Lett.*, *4*, 403–406, 1977.

Kintner, P. M., W. Scales, J. Vago, R. Arnoldy, G. Garbe, and T. Moore, Simultaneous observations of electrostatic oxygen cyclotron waves and ion conics, *Geophys. Res. Lett.*, *16*, 739–742, 1989.

Klumpar, D. M., Transversely accelerated ions: An ionospheric source of hot magnetospheric ions, *J. Geophys. Res.*, *84*, 4229–4237, 1979.

Lennartsson, W., and E. G. Shelley, Survey of 0.1- to 16-keV/*e* plasma sheet ion composition, *J. Geophys. Res.*, *91*, 3061–3076, 1986.

Lockwood, M., J. H. Waite, Jr., T. E. Moore, J. F. E. Johnson, and C. R. Chappell, A new source of suprathermal O^+ ions near the dayside polar cap boundary, *J. Geophys. Res.*, *90*, 4099–4116, 1985.

Lockwood, M., M. F. Smith, C. J. Farrugia, and G. L. Siscoe, Ionospheric ion upwelling in the wake of flux transfer events at the dayside magnetopause, *J. Geophys. Res.*, *93*, 5641–5654, 1988.

Lundin, R., B. Hultqvist, E. Dubinin, A. Zackarov, and N. Pissarenko, Observations of outflowing ion beams on auroral field lines at altitudes of many earth radii, *Planet. Space Sci.*, *30*, 715–726, 1982.

Moore, T. E., C. J. Pollock, R. L. Arnoldy, and P. M. Kintner, Preferential O^+ heating in the topside ionosphere, *Geophys. Res. Lett.*, *13*, 901–904, 1986*a*.

Moore, T. E., M. Lockwood, M. O. Chandler, J. H. Waite, Jr., C. R. Chappell, A. Persoon, and M. Sugiura, Upwelling O^+ ion source characteristics, *J. Geophys. Res.*, *91*, 7019–7031, 1986*b*.

Newell, P. T., and C. I. Meng, The cusp and the cleft/boundary layer: Low-altitude identification and statistical local time variation, *J. Geophys. Res.*, *93*, 14,549–14,556, 1988.

Persoon, A. M., D. A. Gurnett, and S. D. Shawhan, Polar cap electron densities from DE 1 plasma wave observations, *J. Geophys. Res.*, *88*, 10,123–10,136, 1983.

Peterson, W. K., R. D. Sharp, E. G. Shelley, R. G. Johnson, and H. Balsiger, Energetic ion composition of the plasma sheet, *J. Geophys. Res.*, *86*, 761–767, 1981.

Schunk, R. W., and J. J. Sojka, A three-dimensional time-dependent model of the polar wind, *J. Geophys. Res.*, *94*, 8973–8991, 1989.

Sharp, R. D., R. G. Johnson, and E. G. Shelley, Observations of an ionospheric acceleration mechanism producing energetic (keV) ions primarily normal to the geomagnetic field direction, *J. Geophys. Res.*, *82*, 3324–3328, 1977.

Shawhan, S. D., D. A. Gurnett, D. L. Odem, R. A. Helliwell, and C. G. Park, The plasma wave and quasi-static electric field instrument (PWI) for Dynamics Explorer-A, *Space Sci. Instrum.*, *5*, 535–550, 1981.

Shelley, E. G., R. G. Johnson, and R. D. Sharp, Satellite observations of energetic heavy ions during a geomagnetic storm, *J. Geophys. Res.*, *77*, 6104–6110, 1972.

Waite, J. H. Jr., T. Nagai, J. F. E. Johnson, C. R. Chappell, J. L. Burch, T. L. Killeen, P. B. Hays, G. R. Carignan, W. K. Peterson, and E. G. Shelley, Escape of suprathermal O^+ ions in the polar cap, *J. Geophys. Res.*, *90*, 1619–1630, 1985.

Waite, J. H. Jr., T. E. Moore, M. O. Chandler, M. Lockwood, A. Persoon, and M. Sugiura, Ion energization in upwelling ion events, in *Ion Acceleration in the Magnetosphere and Ionosphere, Geophys. Monogr. Ser.*, vol. 38, edited by T. Chang, pp. 61–66, AGU, Washington, D. C., 1986.

Whalen, B. A., W. Bernstein, and P. W. Daly, Low altitude acceleration of ionospheric ions, *Geophys. Res. Lett.*, *5*, 55–58, 1978.

Yau, A. W., B. A. Whalen, A. G. McNamara, P. J. Kellogg, and W. Bernstein, Particle and wave observations of low-altitude ionospheric ion acceleration events, *J. Geophys. Res.*, *88*, 341–355, 1983.

Yau, A. W., B. A. Whalen, W. K. Peterson, and E. G. Shelley, Distribution of upflowing ionospheric ions in the high-altitude polar cap and auroral ionosphere, *J. Geophys. Res.*, *89*, 5507–5522, 1984.

Yau, A. W., E. G. Shelley, W. K. Peterson, and L. Lenchyshyn, Energetic auroral and polar ion outflow at DE 1 altitudes: Magnitude, composition, magnetic activity dependence, and long-term variations, *J. Geophys. Res.*, *90*, 8417–8432, 1985.

Young, D. T., F. Geiss, H. Balsiger, P. Eberhardt, A. Ghielmetti, and H. Rosenbauer, Discovery of the He^{2+} and O^{2+} ions of terrestrial origin in the outer magnetosphere, *Geophys. Res. Lett.*, *4*, 561–564, 1977.

M. O. Chandler, C. R. Chappell, T. E. Moore, and C. J. Pollock, Space Science Laboratory, NASA, Marshall Space Flight Center, AL 35812.

D. A. Gurnett, Department of Physics and Astronomy, University of Iowa, Iowa City, IA 52242.

J. H. Waite, Jr., Department of Space Physics, Southwest Research Institute, 3500 Culebra Road, San Antonio, TX 78284.

(Received January 2, 1990;
revised April 20, 1990;
accepted May 8, 1990.)